Ion-neutral chemical reactions between ultracold localized ions and neutral molecules with single-particle resolution

B. Roth, P. Blythe, H. Wenz, H. Daerr, and S. Schiller
Institut für Experimentalphysik, Heinrich-Heine-Universität Düsseldorf, 40225 Düsseldorf, Germany
(Received 23 January 2006; published 19 April 2006)

Chemical reactions between ultracold $^9Be^+$ ions and room-temperature molecular hydrogen isotopomers and between ultracold H_3^+ ions and room-temperature O_2 have been studied in a laser-cooling ion trap apparatus. For small Coulomb crystals of beryllium ions, reactions can be followed at the single-ion level. We demonstrate characterization of a chemical reaction in which neither one of the reactants nor the product is directly detectable. In this case molecular dynamics simulations were used for the determination of ion numbers from images of the $^9Be^+$ ion ensemble. The observed reaction rates are in agreement with the Langevin ion-neutral reaction theory.

DOI: 10.1103/PhysRevA.73.042712 PACS number(s): 34.50.−s, 32.80.Pj, 42.50.−p

I. INTRODUCTION

Chemical reactions between trapped molecular ions and neutral reactants are of significant interest to chemistry and astrophysics, and have been studied for many years at low temperatures. Multipole ion traps using neutral buffer gas as coolant have been used to reach temperatures down to 10 K, see, e.g., [1]. Reaction rates and branching ratios were deduced by extraction of the reaction products from the trap and counting, see [2] for examples.

It is desirable to extend such studies to state-specific reactions, which implies the necessity to prepare the reactants in particular quantum states and with well-defined collision energy. This requires a well-controlled environment in which undesired interactions and transitions between states are minimized. The ability to conduct and observe chemical reactions at the level of individual molecules in a cold, UHV environment has the potential to improve our understanding of important astrochemical reactions [3–5], through improvements in the accuracy of measurements of reaction rates and branching ratios [6], and by using narrow-bandwidth lasers to study chemical reactions state-selectively.

Regarding the ion side of this challenging program, significant progress was made in recent years in the generation of ensembles of ultracold (<1 K) pure and mixed-species ion plasmas in traps using laser cooling techniques. In particular, sympathetic cooling by laser-cooled atomic ions was used to cool ion species which cannot be directly laser cooled due to the lack of closed optical transitions. Various atomic and molecular ion species covering a broad mass range have been cooled to milliKelvin temperatures and brought to rest inside ordered structures, denoted by Coulomb crystals [7–10]. In these crystals the ions are located in well-defined shell structures. At the lowest temperatures reached (<10 mK) the ions remain mostly confined in the immediate vicinity of their equilibrium positions.

The next important development required in order to reach complete state preparation is internal cooling, i.e., population of a particular rovibrational level. This goal can be reached by collisions with cold neutral buffer gas and, possibly, laser cooling techniques. Such translationally and internally ultracold ensembles will be an important ingredient in the study of gas phase ion-neutral reactions and collision processes at the quantum level.

Thus far, a first study of chemical reactions with one ultracold partner has been demonstrated: chemical reactions between large ensembles of laser-cooled and crystallized Ca^+ ions, excited to the $^2P_{1/2}$ state, and neutral molecular oxygen gas at 300 K were investigated and reaction rates extracted [11]. Subsequently, the reaction products formed, CaO^+ ions, were exposed to 300 K neutral CO and reacted back to Ca^+ and CO_2. This reaction has been observed with sensitivities down to the single particle level [12]. Furthermore, ion-neutral reactions in which the molecular ions were sympathetically cooled to 10 K by laser-cooled Mg^+ ions were studied [13]. The reaction was detected by using the laser-cooled ions for monitoring the decrease of the reactant molecular ions, via mass spectroscopy.

In the present work we extend the works of Refs. [11,13] in several directions: (i) small ensembles, which could be interesting systems for quantum state preparation, (ii) reactions with the simplest molecules which are most easily amenable to *ab initio* calculation and which are of astrophysical importance, (iii) reactions in which the laser-cooled atomic ions in crystals are "spectators" only—thereby demonstrating that it is possible to detect and measure reactions in which neither one of the reactants nor the product is directly detectable, and (iv) employing MD simulations rather than mass spectroscopy for interpreting the observations and determining the reactant number decrease.

A first set of studied chemical reactions is between laser-cooled $^9Be^+$ ions and neutral molecular hydrogen isotopomers. Secular excitation mass spectroscopy was used to identify the reaction products. The reaction rates were deduced from the time evolution of the Be^+ ion number and/or of the spontaneous emission fluorescence rate, recorded by a CCD camera. The available reaction channels for this system are [14]

$$Be^+ + XY \rightarrow BeX^+ + Y \quad (1)$$

$$\rightarrow BeY^+ + X \quad (2)$$

$$\rightarrow \mathrm{Be}X + Y^+ \tag{3}$$

$$\rightarrow \mathrm{Be}Y + X^+ \tag{4}$$

$$\rightarrow \mathrm{Be} + XY^+, \tag{5}$$

where $\{X,Y\} \in \{\mathrm{H},\mathrm{D}\}$. These reactions do not proceed with the beryllium ion in its ground electronic state. For example, the reaction

$$\mathrm{Be}^+(^2S_{1/2}) + \mathrm{H}_2(X^1\Sigma_g^+) \rightarrow \mathrm{BeH}^+(X^1\Sigma^+) + \mathrm{H}(^2S_{1/2}) \tag{6}$$

is endothermic by 1.57 eV [14]. Similar values hold when replacing H_2 by HD or D_2. The endothermicities of the other possible reaction channels are: 2.45 eV for reactions 3 and 4, and 1.9 eV for reaction (5). Therefore, the Be^+ ion must be excited, e.g., to the $^2P_{3/2}$ state (by 3.9 eV photons) in order to react. However, we do not observe reactions (3), (4), and (5) even when Be^+ is electronically excited in our trap, probably due to the large kinetic energy transferred to the reaction products, H^+, D^+, or HD^+, leading to their loss from the trap.

The Be^+ ions in these experiments are continuously laser-cooled by a 313 nm all-solid-state laser system [15], and this simultaneously provides the (partial) excitation necessary for the reactions to proceed. By altering the intensity or detuning of the cooling laser, we can modify the excitation rate and hence the reaction rate, allowing for control of the process.

In mixed-species ion crystals containing laser-cooled (LC) Be^+ ions and sympathetically cooled (SC) triatomic hydrogen molecular ions, H_3^+, we have studied the reaction

$$H_3^+ + O_2 \rightarrow HO_2^+ + H_2 \tag{7}$$

and deduced the corresponding reaction rate. This reaction is nearly thermoneutral, see [18], and references therein. However, the reaction rates for the back reaction $HO_2^+ + H_2 \rightarrow H_3^+ + O_2$ were found to be smaller than for the forward direction [19].

The Langevin theory of ion-neutral reactions predicts, for suitably low temperatures, a reaction rate which is independent of temperature [16,17]. The reaction rate for beryllium ions in reactions (1)–(5) or H_3^+ ions in reaction (7) is given by

$$R_L = -dN_i(t)/dt = -k_L N_n N_i(t), \tag{8}$$

where N_i denotes the ion number, N_n is the (constant) number density of neutral reactants, and $k_L = -23.42\sqrt{\alpha/\mu} \times 10^{-10}$ cm^3/s is the Langevin coefficient. α is the polarizability of the neutral reactant and μ is the reduced mass of the reacting particles. For an initial ion number $N_{i,0}$ at time $t=0$ the number of remaining ions $N_i(t)$ is

$$N_i(t) = N_{i,0} e^{-k_L N_n t}. \tag{9}$$

II. EXPERIMENTAL SETUP

We use a linear radio-frequency trap to simultaneously store both Be^+ and sympathetically cooled ions, e.g., H_3^+ ions. The trap is driven at $\Omega/2\pi = 14$ MHz, with a peak-to-peak amplitude $2V_{\mathrm{RF}} = 380$ V and is enclosed in an UHV chamber kept below 10^{-10} mbar. The chamber is equipped with a leak valve for the controlled introduction of gases, whose partial pressure is controlled by a quadrupole mass analyzer and an ion gauge.

Typically, we set the radial Mathieu stability parameter, $q = 2QV_{\mathrm{RF}}/m\Omega^2 r_0^2 \simeq 0.054$ for the Be^+, giving a radial secular oscillation frequency ("single particle frequency"), $\omega_r = (\omega_0^2 - \omega_z^2/2)^{1/2} \simeq 280$ kHz [9]. Q and m are the charge and the mass of the ions, $r_0 = 4.3$ mm is the distance from the trap center to the electrodes, and $\omega_0 = QV_{\mathrm{RF}}/\sqrt{2}m\Omega r_0^2$. The longitudinal frequency $\omega_z = (2\kappa QV_{EC}/m)^{1/2}$ is determined by the static potential V_{EC} applied to the end sections of the trap to achieve confinement of the ions in the z direction. κ is a constant determined by the trap geometry. For the molecular hydrogen ions q lies between 0.162 (H_3^+) and 0.240 (H_2^+).

The trapped ion species are identified by the spectroscopy of their motional frequencies. For this purpose, we excite the ions' motion in the time-averaged effective potential using an additional plate electrode between the two uppermost trap electrodes (at 45° to the x and y axes of the trap, parallel to the z axis). An oscillating potential is applied to the electrode, at frequencies between 2 kHz and 3 MHz, and with an amplitude up to 10 V. The frequency of the excitation is scanned, while the Be^+ fluorescence is recorded. When the applied frequency is resonant with a motional frequency of a species in the crystal, that motion is excited, the ions are heated, and the fluorescence of the beryllium ions in the crystal is affected. The heating of the crystal causes an increase in fluorescence when the cooling laser is detuned sufficiently to the red of the cooling transition.

To load Be^+ ions into the trap, atoms are thermally evaporated from a beryllium wire, and ionized in the trap center by a 750 eV electron beam. This produces a large cloud of beryllium ions, along with impurities from ionization of background gas present in the vacuum chamber. The heavier impurities can be removed by temporarily applying a static quadrupole potential to the trap such that it becomes unstable for elements with a higher mass-to-charge ratio than that of Be^+.

For laser cooling of Be^+ ions we produce circularly polarized light resonant with the $^2S_{1/2}(F=2) \rightarrow {}^2P_{3/2}$ transition at 313 nm. The UV laser light is frequency stabilized to a hyperfine transition of molecular iodine. An acousto-optic modulator (AOM) allows us to shift the UV frequency within a range of 370 MHz while maintaining absolute frequency stability. Spontaneous emission to the metastable ground state $^2S_{1/2}(F=1)$ is prevented using a repumper red detuned by 1.250 GHz. The laser cooling beam is parallel to the symmetry axis (z axis) of the trap. For definition of a quantization axis, magnetic fields in the few Gauss range are applied to the trap parallel to z.

III. METHOD

A. Preparation of ultracold pure and mixed-species ion crystals

Ensembles of Be^+ ions are produced, trapped, and subsequently laser-cooled so that they undergo a phase transition

to an ordered state, a Coulomb crystal [20]. Typically, the crystals studied here have translational temperatures of ≈ 10 mK, as found by measurement of the spontaneous emission fluorescence line shape and confirmed by molecular dynamics (MD) simulations [10,21]. When required, light molecular ions, e.g., molecular hydrogen isotopomers, are produced via electron impact ionization of neutral gas introduced to the vacuum chamber at pressures of approximately. 4×10^{-10} mbar. The loading rate is controlled by the partial pressure of the gas and the electron beam intensity. As a consequence of trapping and sympathetic crystallization of the molecular ions a dark inner region evolves in the initially pure Be^+ crystals. The lighter molecular species experience a stronger effective potential inside the trap and are therefore embedded closer to the symmetry axis of the trap. Usually, during the loading of molecular hydrogen ions into the trap, various lighter impurities (molecular hydrogen isotopomers) are produced by chemical reactions together with the species under study. Such impurities are removed by melting the crystal and subsequently exciting the resonant motion of a particular ion species at sufficiently large excitation amplitudes. This leads to the ejection of that particular species while leaving nearly undisturbed the species under study. The ion cloud is then recrystallized and a two-species ion crystal is obtained [9].

B. Measurements

The above pure or mixed-species Be^+ ion crystals are the starting point for our studies. Since the reaction rate between LC Be^+ ions and hydrogen isotopomers depends on the relative population of the $^2P_{3/2}$ state in Be^+, prior to each measurement the fraction of excited Be^+ ions is determined. For this purpose, the cooling laser is tuned to maximum fluorescence, which corresponds to a relative population of the upper level of 50% (the laser intensity $I \approx 10$ mW/mm^2 is much larger than the saturation intensity $I_{sat}=0.8$ mW/cm^2), and the corresponding photon count rate recorded by a photomultiplier tube (PMT) is used for calibration. A particular level of excitation can be set by frequency-detuning the cooling laser to the red side of the atomic resonance using an AOM.

Subsequently, neutral reactants are leaked into the vacuum chamber at typical pressures between 2×10^{-10}–2×10^{-9} mbar. At these pressures the Langevin theory should still apply [17]. After the partial pressure of the introduced neutral reactant has reached a constant value the Be^+ fluorescence is recorded both with a PMT and with a charge-coupled device (CCD) camera as a function of time. In these measurements the PMT has a time resolution of 0.1 s, whereas the camera exposure time typically is in the range of 0.5–2 s.

The ion species involved were identified by secular excitation mass spectrometry, as described above. The chemical reaction process can be stopped at any time by closing the leak valve, and secular scans can be made to determine the presence of reaction products, e.g., BeH^+ and BeD^+. Individual features in the measured mass spectra were assigned to the different ion species contained in the crystal by comparison with spectra obtained from MD simulations, see also [21,22].

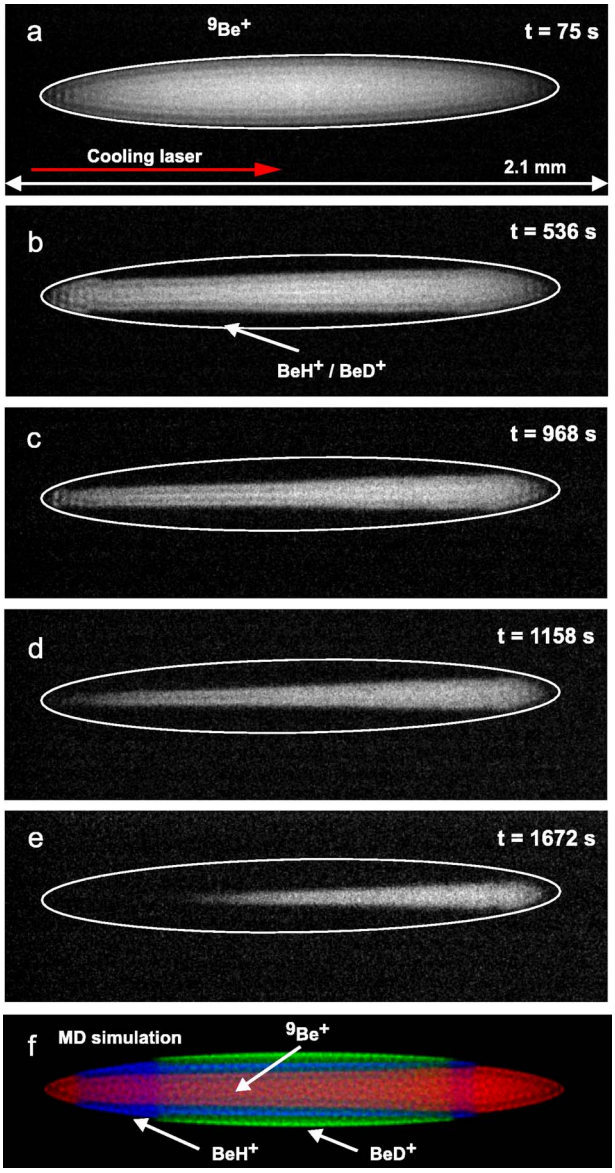

FIG. 1. (Color online) CCD camera image of an initially pure large Be^+ ion crystal following exposure to HD gas, leading to the formation of ultracold BeH^+ and BeD^+ molecular ions via chemical reactions. The ellipse is a fit to the initial Be^+ crystal boundary. The molecular ions formed are located in the dark area enclosed. The ion numbers determined using MD simulations are: (a) 2100 Be^+, (b) 900 Be^+, 1200 BeH^+ and BeD^+ (in approx. equal amounts), (c) 500 Be^+, 1600 BeH^+ and BeD^+, (d) 310 Be^+, 1700 BeH^+ and BeD^+, (e) 150 Be^+, 1700 BeH^+ and BeD^+. (f) MD simulation of the crystal in (b), with 900 Be^+ and 600 BeH^+ and BeD^+ ions, respectively, at approximately 15 mK.

During exposure to neutral hydrogen gases the observed Be^+ ion crystal changes its shape, as a consequence of the formation and sympathetic crystallization of BeH^+ and BeD^+, embedded in the outer regions of the crystal. For the example shown in Fig. 1, an initially pure Be^+ crystal (a) was exposed to neutral HD gas and its structural changes were observed as function of time, (b)–(e). A marked increase in

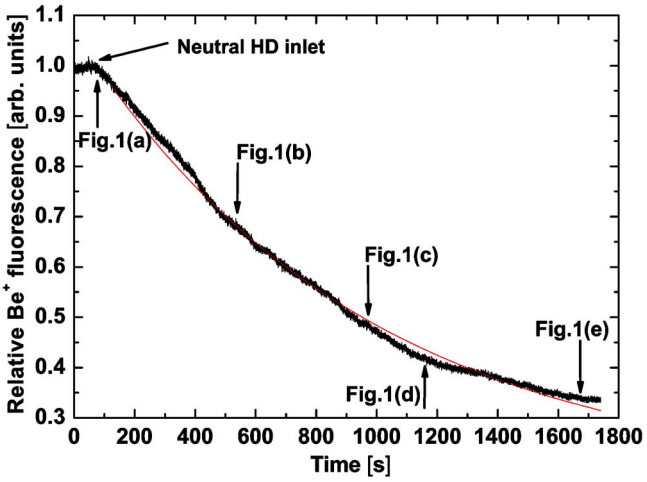

FIG. 2. (Color online) Decay of a Be^+ ion crystal containing initially ≈2100 Be^+ ions after exposure to HD gas. Relative population of the $^2P_{3/2}$ level of Be^+: 0.14. The line is an exponential fit to the data. CCD camera images in Fig. 1 were taken at the indicated times.

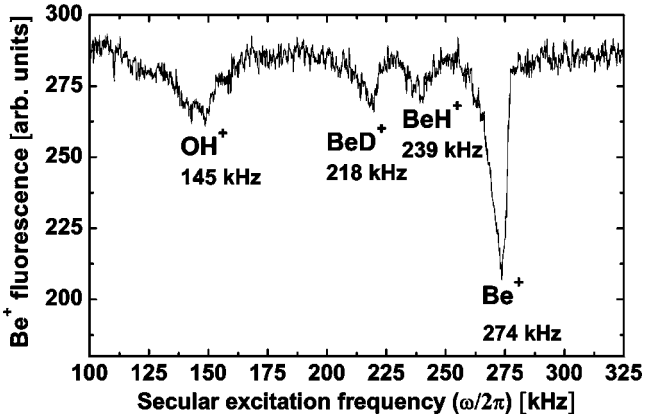

FIG. 3. Motional frequency spectrum for a laser-cooled Be^+ plasma after exposure to neutral HD gas. The spectrum was taken with the mixed-species plasma in the cloud state. The measured secular frequencies agree well with the calculated single-particle secular frequencies.

the temperature of the Be^+ ensemble is observed. The Be^+ ion temperature is determined by a balance between the (laser) cooling rate and the heating rate. The heating rate has a contribution arising from the SC particles, which are heated by collisions with background gas and by rf heating in the trap due to ion-ion interactions. This contribution becomes more important as the number of SC ions increases and the number of LC ions decreases. The translational temperature of the initially pure Be^+ crystal of ≈10 mK (a) increased to ≈40 mK (e) during the reaction. Thus, the increased Be^+ ion temperature directly reflects the formation of ultracold molecular ions. Also, due to the reduction of sympathetic cooling power a part of the molecular ions produced is lost from the trap. The observed lack of symmetry of the mixed-species crystal shape with respect to the *x*-*y* plane is due to the presence of the SC particles combined with the laser light pressure force that is exerted only on the LC particles. As the chemical reactions proceed in time, the total fluorescence rate of the Be^+ ions decreases, see Fig. 2.

A typical secular frequency spectrum obtained for the reaction is shown in Fig. 3. The spectrum was taken several minutes after exposing a Be^+ ion crystal to neutral HD with the ion ensemble in the cloud state. In this state the interpretation of the mass spectrum is much simpler than in the crystal state due to the reduction of interspecies coupling effects [22]. Ionic species with small differences of their mass-to-charge ratio can then be resolved more easily, e.g., Be^+, BeH^+, and BeD^+.

The spectrum shows three pronounced features stemming from LC (Be^+, 275 kHz) and SC particles (BeH^+, 248 kHz; BeD^+, 225 kHz). The calculated single-particle secular frequencies for the above species are 275 kHz (Be^+), 248 kHz (BeH^+), and 225 kHz (BeD^+), in good agreement with the experimental observation. An additional feature is obtained at 145 kHz, stemming from sympathetically cooled OH^+ ions. OH^+ impurity ions are formed during Be^+ loading by electron-impact ionization of residual background H_2O molecules present in the vacuum chamber. Usually, prior to each measurement, such impurity ions are removed from the crystal, as described above.

The reaction of individual LC Be^+ ions with neutral molecular hydrogen gases can be observed as a function of time by either sudden jumps in the detected spontaneous emission fluorescence signal or by the disappearance of individual ions. This requires small ion ensembles. In Fig. 4(a) the fluorescence decay curve of a small Be^+ ion crystal (160 Be^+ ions) exposed to neutral HD gas is shown together with corresponding CCD images. The chemical reactions can indeed be followed with single particle resolution. Once the ion number has decreased so far that the Be^+ ions are arranged in a string discrete jumps in the fluorescence decay curve can be identified, which are correlated with the production of single molecular ions, see Fig. 4(b).

The reaction $H_3^+ + O_2 \rightarrow HO_2^+ + H_2$ was studied in a similar way. H_3^+ molecular ions are produced in a two-step process. First, H_2^+ ions are formed via electron impact ionization of neutral H_2 gas and embedded in the Be^+ ion crystal. Subsequently, the ions produced react with neutral H_2 via $H_2^+ + H_2 \rightarrow H_3^+ + H$ [10]. Figures 5(a)–5(c) show an initial two species ion crystal containing Be^+ and H_3^+ (a), which is exposed to neutral O_2 gas. As a consequence of the chemical reactions ultracold HO_2^+ ions are formed and the H_3^+ dark core disappears, Figs. 5(b) and 5(c). MD simulations of the mixed-species ion crystals in Figs. 5(a) and 5(c) are presented in Figs. 5(d) and 5(e), respectively. Since the structure of the simulated crystal is quite sensitive to the mass-to-charge ratio and the number of ions of each species, see also [21], the reproduction of the observed crystal shape by the simulations represents a first (indirect) identification of the produced species. The comparison between experimental images and simulated crystal structures allows for an estimate of the conversion efficiency of initial H_3^+ ions into HO_2^+ during exposure to molecular oxygen. We find that essentially all H_3^+ ions react with neutral O_2 and that the reaction products formed, HO_2^+, remain trapped and embedded in an outer "belt."

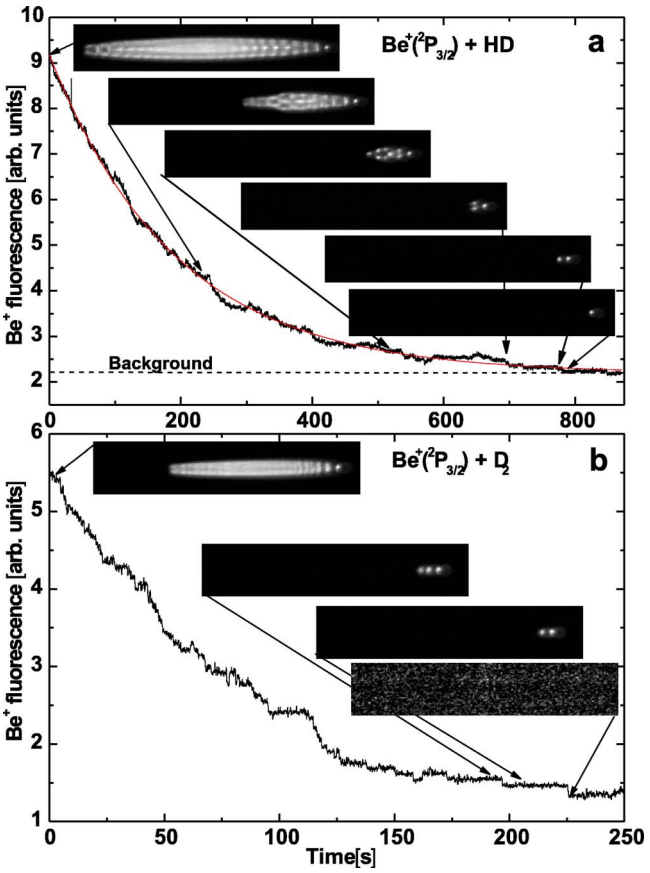

FIG. 4. (Color online) Decay of a small Be^+ ion crystal initially containing ≈160 Be^+ at ≈5 mK after exposure to neutral HD gas. Relative population of the $^2P_{3/2}$ level of Be^+: 0.42. The line is an exponential fit to the data. (b) Decay of a crystal containing initially ≈45 Be^+ ions after exposure to D_2 gas. Towards the end of the record two discrete steps in the fluorescence due to the formation of a single BeD^+ ion, and of two BeD^+ ions, respectively, are observed. Relative population of the $^2P_{3/2}$ level of Be^+: 0.23.

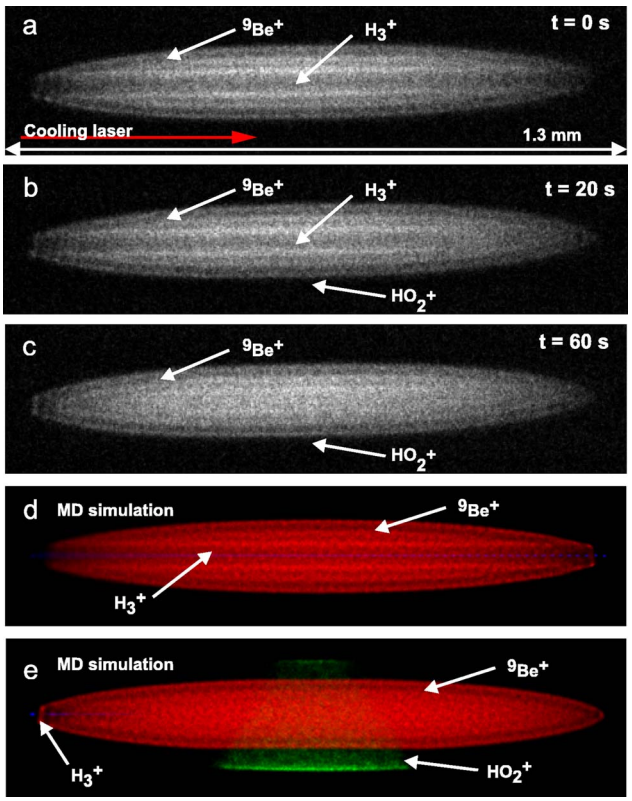

FIG. 5. (Color online) (a)–(c) Images of an initially pure Be^+-H_3^+ ion crystal exposed to neutral O_2 at 3×10^{-10} mbar. H_3^+ disappears from the crystal core as HO_2^+ molecules are formed and embedded in the outer region of the crystal. Their presence leads to a slight flattening of the upper and lower edge of the crystal in image (c). (d) MD simulation of the crystal in (a) containing 1275 Be^+ and 80 H_3^+ ions at ≈30 mK. (e) MD simulation of the crystal in (c) containing 1275 Be^+, 3 H_3^+, and 75 HO_2^+ ions at ≈30 mK.

Direct identification is illustrated in Figs. 6(a)–6(c) where the secular excitation spectra for the mixed species ion crystal in Figs. 5(a) and 5(c) are shown. The secular excitation spectra in Figs. 6(a) and 6(b) were taken after loading of the H_3^+ into the crystal. Whereas the low mass secular scan (a) evidences the presence of H_3^+ ions, particles with mass-to-charge ratio larger than Be^+ are absent (b). The rise of the Be^+ fluorescence in Fig. 6(b) towards the end of the scan is due to excitation of the nearby (at 280 kHz) radial Be^+ trap mode by the large excitation amplitude used. The appearance of HO_2^+ ions is observed after the exposure of the Be^+-H_3^+ ion crystal to neutral molecular oxygen, Fig. 6(b). According to the simulations the translational temperature of LC and SC particles is at ≈30 mK.

C. Analysis

The number of particles as a function of reaction time was determined by performing MD simulations corresponding to various time instants. The temperature of the SC particles was also determined by the simulations, see [9,21]. The size of the imaged ion fluorescence spots is compared to the simulation results leading to an estimate for the temperature of the LC particles. Due to the Coulomb interaction between LC and SC ions the temperature of the SC ions also influences the temperature of the LC ions, and thus, the ion structures observed. Therefore, from the temperature of the LC particles we can set upper limits for the SC temperature. The observed ion shell structures are consistent with a SC temperature well below 15 mK. The simulations show that, if the temperature of the SC particles embedded in the outer region of the crystal is kept at ⩾50 mK, the Be^+ ion shells close to the molecular ions would appear much more blurred, in contrast to observation. Tighter upper limits can be set by considering the balance between heating and cooling rates relevant for the SC particles. Typically, for the crystals studied here, the temperature of the SC ions is within a factor of 2 of the LC temperature.

While secular excitation mass spectroscopy is suitable to reliably detect LC and SC ion species in the produced crystals, it is not easily made quantitative, and thus, reaction rates cannot be determined by the size of the spectral features. In general, mass spectroscopy in large and mixed-species ion crystals is complicated by coupling between the trap oscillation modes of different species, induced by Coulomb inter-

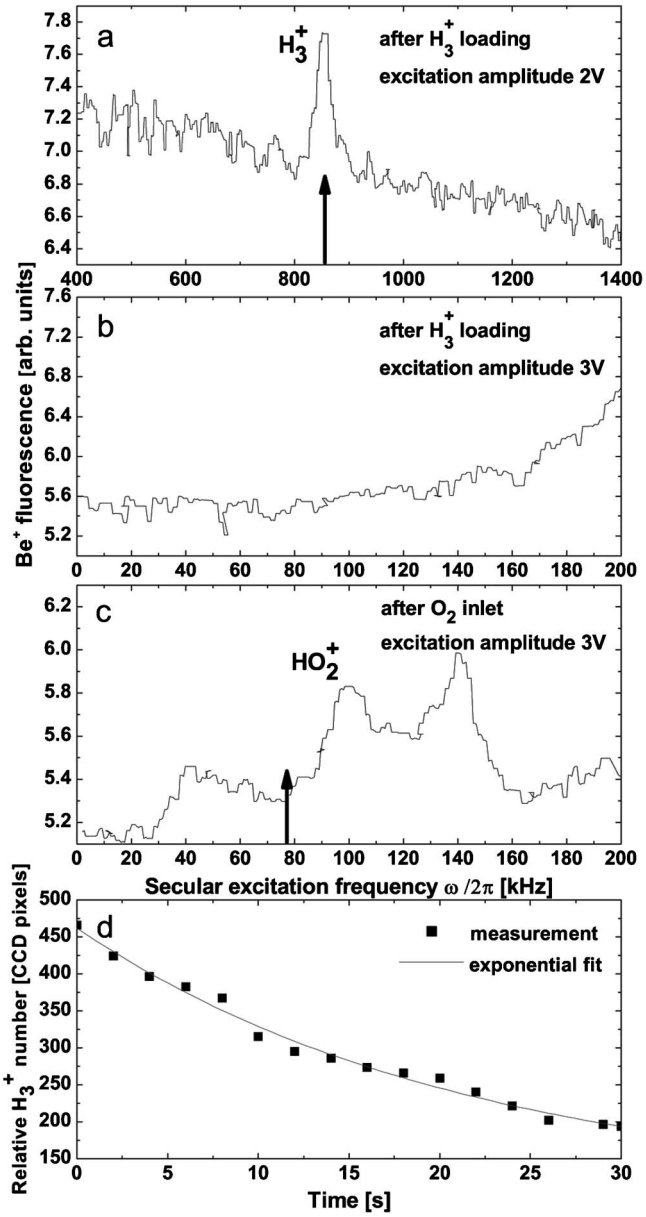

FIG. 6. Secular frequency spectrum of the crystal shown in Fig. 5 after loading of H_3^+ ions. (a) Low-mass range and (b) high-mass range. (c) shows the spectrum of the crystal after exposure to O_2 molecules, Fig. 5(c). The feature at around 100 kHz originates from the HO_2^+ ions formed. The calculated single-particle secular frequencies for H_3^+ and HO_2^+ are indicated by arrows. Due to the Coulomb coupling between the particles the measured frequency is shifted toward larger values [21,22], as confirmed by the simulations. The feature at around 50 kHz is due to the excitation of the axial Be^+ oscillation mode, see [26]. The feature at 140 kHz originates from a composite HO_2^+-Be^+ mode. (d) Relative H_3^+ number for the reaction $H_3^+ + O_2 \rightarrow HO_2^+ + H_2$ for the crystal shown in Figs. 5(a)–5(c). The H_3^+ number was derived by analyzing the decrease of the dark crystal core containing H_3^+ ions after exposure to neutral O_2.

action [22–25]. Instead, fluorescence detection or direct "ion counting" using CCD images allows for precise measurements of reaction rates with single particle sensitivity. In this

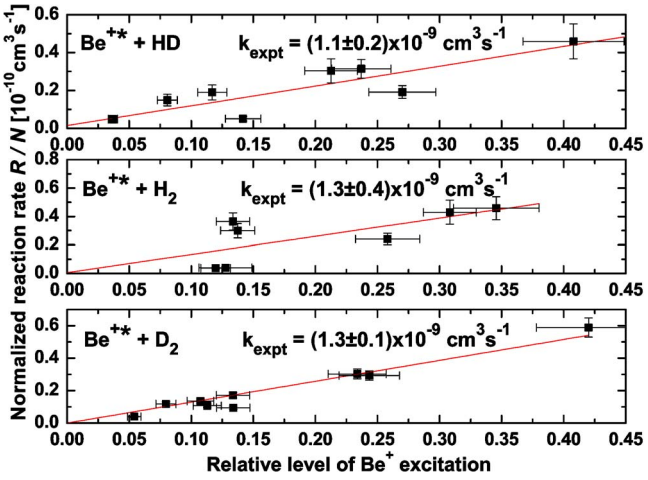

FIG. 7. (Color online) Normalized reaction rates per particle for the chemical reactions of excited Be^+ with H_2 (a), HD (b), and D_2 (c) as a function of the level of excitation. The reaction rates R were obtained from least-squares exponential fits of the Be^+ fluorescence rate versus time. The lines are linear fits to the data. The reaction coefficient k_{expt} is obtained from the slope of the fits.

work, fluorescence detection is used for crystals with large numbers of Be^+ ions, enabling a good signal to noise ratio, whereas for small and medium sized crystals (with ion numbers from a few ions up to several hundred) ion counting is more suitable. The latter has the potential for precise reaction rate measurements with good signal to noise ratio and almost no background events.

Reaction rates for the chemical reactions observed are obtained by least-squares fitting the fluorescence decay or particle loss curves versus time. Reactions were measured as a function of the excitation level and the partial pressure of the neutral gases. The corresponding Langevin coefficients are deduced by normalizing the reaction coefficients to the neutral reactant particle number density and the excitation level.

For the reactions between ultracold H_3^+ ions and neutral O_2 gas the reaction coefficient is deduced from least-squares fitting to the hydrogen ion loss rate. The latter is obtained from the CCD images by analyzing the decrease of the dark core as a function of time, see Fig. 6(d). The reaction coefficient is then determined in the same way as above, except that the excitation level of the Be^+ ions is irrelevant here.

IV. RESULTS AND DISCUSSION

Figure 7 shows the reaction rates R for the chemical reactions described in Eq. (1), normalized by the particle number density N_n for H_2 (a), HD (b), and D_2 (c) as a function of the level of excitation. These reaction rates were obtained from least-squares fitting of the logarithm of the Be^+ fluorescence curve versus time. The main uncertainties for the measurements presented are the uncertainty of neutral reactant number density N_n and the uncertainty associated with the determination of the level of Be^+ excitation, both included in Fig. 7 for each data point. For the measurements shown, the errors of N_n are below 10%. Systematic errors stemming from Be^+ losses upon reaction with residual hydrogen gas are

TABLE I. Experimental and Langevin reaction coefficients and experimental uncertainties Δk_{expt}. The values for the electric dipole polarizabilities used in Eq. (8) to obtain k_L are (in units of 10^{-24} cm^3): 0.8042 (H_2), 0.7976 (HD), 0.7921 (D_2), and 1.5812 (O_2) [27].

Reaction	k_{expt} (cm^3/s)	Δk_{expt} (cm^3/s)	k_L (cm^3/s)
$Be^+ + H_2$	1.3×10^{-9}	0.4×10^{-9}	1.6×10^{-9}
$Be^+ + HD$	1.1×10^{-9}	0.2×10^{-9}	1.4×10^{-9}
$Be^+ + D_2$	1.3×10^{-9}	0.1×10^{-9}	1.3×10^{-9}
$H_3^+ + O_2$	1.1×10^{-9}	0.4×10^{-9}	1.7×10^{-9}

negligible for our experimental conditions. The slopes of the fitted lines in Fig. 7 give the reaction coefficients, and are summarized in Table I. The relative reaction rates have somewhat smaller uncertainties than the absolute reaction rates due to uncertainty in the absolute calibration of the ion gauge used. The reaction coefficients for the reactions studied are comparable to the Langevin values [Eq. (8)], which are all in the same range.

In Fig. 8 the measured reaction rates for the chemical reaction $H_3^+ + O_2 \rightarrow HO_2^+ + H_2$ are shown. The reaction rates were deduced from the CCD camera pictures by analyzing the H_3^+ loss rate as the rate of dark crystal core size reduction. From the analysis of the CCD camera images we obtain the particle loss rate in pixels/s which is translated into particles/s via the MD simulations. This can be done with an accuracy at the single ion level. The main uncertainties in this measurement come from estimating the particle number density N_n ($<10\%$). Systematic errors due to reactions between H_3^+ and background hydrogen gas are below $(7.5\pm) \times 10^{-3}$/s. The rate coefficient is obtained from the linear fit to the experimental data, and is listed in Table I.

The measured rate coefficients for all reactions studied are in reasonable agreement with the values calculated from Langevin theory. The uncertainties shown in Table I can be attributed to calibration errors of the ion gauge used, which is relevant here because of the low reactant pressures used, and the uncertainty in the laser excitation rate.

A reliable estimate of the number of SC ions of various species within a Coulomb crystal from the secular excitation spectrum is not (yet) available. Possibly, structural details might be used to determine ion numbers of SC species

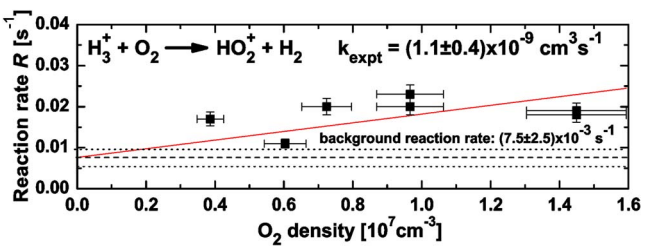

FIG. 8. (Color online) Reaction rates for the reaction $H_3^+ + O_2 \rightarrow HO_2^+ + H_2$ versus O_2 particle number density N_n. The line is a linear fit to the experimental data. The reaction coefficient k_{expt} is obtained from the slope of the fit. The main uncertainties come from the measured particle number densities N_n.

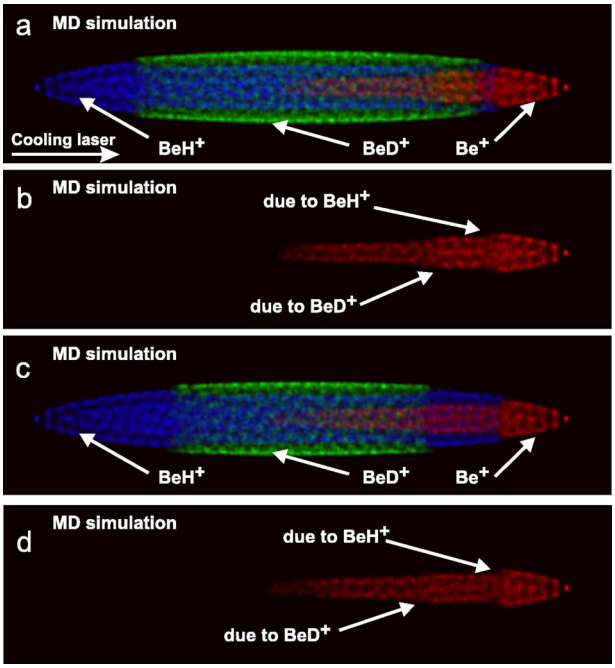

FIG. 9. (Color online) (a) Simulated Be^+ ion crystal containing 100 Be^+, 300 BeH^+, and 300 BeD^+ ions at $\approx$10 mK. (b) Same as in (a), only LC particles are displayed. Be^+ ions are shifted to the right by light pressure forces. The distortions in the outer Be^+ shell, induced by SC particles, are marked. (c, d) Simulated Be^+ ion crystal containing 100 Be^+, 400 BeH^+, and 200 BeD^+ ions at $\approx$10 mK. The difference between the distortions in (b) and (d) might allow for a species-selective estimate of SC ion numbers.

heavier than the LC ions. We find that in medium-size crystals each SC species present in the outer layers of the crystal has a detectable effect on the shape of the Be^+ ion crystal boundary. As an example, in Fig. 9 we compare two simulated trispecies Be^+ ion crystals with a different BeH^+/BeD^+ number ratio. The Be^+ ions are shifted relative to the SC particles by light pressure forces included in the simulations. The presence of the two SC species, BeH^+ and BeD^+, induces two "ridges" in the Be^+ structure because of the different effective trap potential for the two SC species. The position of the ridges and the details of the Be^+ ion crystal structure are functions of the individual SC ion numbers. Thus, a systematic experimental study of the LC crystal structure as a function of the laser light pressure force and comparison with MD simulations might allow for a species-selective estimate of SC ion numbers.

V. SUMMARY AND OUTLOOK

The results presented in this work represent a novel example of the use of laser-manipulated particles for chemical reaction studies. Using the method described chemical reactions between ultracold ensembles of selectable initial ion number from a few up to several thousand particles can be observed as a function of time.

We have observed chemical reactions between laser-cooled, excited Be^+ ions and neutral H_2, HD, and D_2 molecules. Measurements of reaction rates from the study of

CCD images and laser-cooling fluorescence levels are in agreement with the Langevin ion-neutral reaction model. Furthermore, we have studied chemical reactions between ultracold triatomic hydrogen molecules, H_3^+, sympathetically cooled by laser-cooled Be^+, and molecular oxygen. In this reaction, MD simulations were an important tool, allowing us to determine the number of ions of one of the reaction partners and to deduce upper limits for the translational temperature of the particles. Thus we have shown that is is possible to study certain chemical reactions even in the case when neither one of the reactants nor the products can be directly detected.

Ultracold laser-cooled and sympathetically cooled ions in traps open up the possibility for high-precision measurements on well-localized systems and are interesting targets for the study of chemical reactions of atoms and molecules interesting to astrophysics and chemistry. The method presented has the potential to observe chemical reactions at the level of individual molecules in a cold environment.

Returning to the perspective outlined in the Introduction, the study of chemical reactions between state-prepared ultracold atomic/molecular ions and state-prepared ultracold neutral molecules, we point out that the preparation of translationally ultracold ensembles are by now established techniques both on the ion side and on the neutral side. Translationally ultracold neutral molecules can be generated by a number of techniques, such as, photoassociation, Feshbach resonances in optical traps [28,29], Stark deceleration and subsequent trapping by time-varying electric fields [30], filtering out of a thermal ensemble and storage in a electrostatic quadrupole trap [31], or cryogenic buffer gas cooling possibly followed by magnetic trapping [32]. The challenging next tasks are the combination of these and molecular ion state preparation techniques into a single apparatus.

Another interesting perspective is the generation and use of mixed-species ion strings with deterministic order. Ordering might be achieved starting with an initially pure Be^+ ion string, switching off the laser cooling, and subsequently illuminating only individual Be^+ ions by the same laser, tightly focused on the particular ion. Injection of neutral molecular hydrogen would then lead to the formation of a molecular ion at a desired position in the string. Such two-species linear ion chains could be used to implement new cooling schemes for the vibrational motion of extended linear ion chains or to prepare molecular quantum states for quantum information processing (see [33] and references therein). Furthermore, quantum logic techniques could be used to study the vibrational trap mode spectrum of mixed-species ion chains containing sympathetically cooled particles [34].

ACKNOWLEDGMENTS

The authors thank U. Fröhlich for contribution to the initial phase of this work, the Deutsche Forschungsgemeinschaft (DFG) and the EU network HPRN-CT-2002-00290 "Ultracold Molecules" for financial support. P.B. was supported by the EU network and the Alexander-von-Humboldt Stiftung.

[1] D. Gerlich, *Advances in Chemical Physics: State-Selected and State-to-State Ion Molecule Reaction Dynamics* (Wiley, New York, 1992), Vol. LXXXII.
[2] D. Gerlich, E. Herbst, and E. Roueff, Planet. Space Sci. **50**, 1275 (2002); O. Asvany, I. Savic, S. Schlemmer, and D. Gerlich, Chem. Phys. **298**, 97 (2004).
[3] E. Herbst, Philos. Trans. R. Soc. London, Ser. A **358**, 2523 (2000).
[4] T. Glenewinkel-Meyer and D. Gerlich, Isr. J. Chem. **37**, 343 (1997).
[5] See, e.g., Philos. Trans. R. Soc. London, Ser. A **358**, Nr. 1774 (2000); J. Mikosch *et al.*, J. Chem. Phys. **121**, 11030 (2004).
[6] A. Bertelsen, I. S. Vogelius, S. Jørgensen, R. Kosloff, and M. Drewsen, Eur. Phys. J. D **31**, 403 (2004).
[7] D. J. Larson, J. C. Bergquist, J. J. Bollinger, W. M. Itano, and D.. J. Wineland, Phys. Rev. Lett. **57**, 70 (1986).
[8] P. Bowe, L. Hornekaer, C. Brodersen, M. Drewsen, J. S. Hangst, and J. P. Schiffer, Phys. Rev. Lett. **82**, 2071 (1999).
[9] B. Roth, U. Fröhlich, and S. Schiller, Phys. Rev. Lett. **94**(5), 053001 (2005).
[10] P. Blythe, B. Roth, U. Fröhlich, H. Wenz, and S. Schiller, Phys. Rev. Lett. **95**, 183002 (2005).
[11] L. Hornekær, Ph.D. thesis, Aarhus University (2000).
[12] M. Drewsen, L. Hornekaer, N. Kjaergaard, K. Molhave, A. M. Tommensen, Z. Videnseu, A. Mortensen, and F. Jensen, in *Non-Neutral Plasma Physics Conference IV*, AIP Conf. Proc. No. 606 (AIP, New York, 2002), p. 135.
[13] T. Baba and I. Waki, J. Chem. Phys. **116**, 1858 (2002).
[14] M. Raimondi and J. Gerratt, J. Chem. Phys. **79**(9), 4339 (1983).
[15] H. Schnitzler, U. Fröhlich, T. K. W. Boley, A. E. M. Clemen, J. Mlynek, A. Peters, and S. Schiller, Appl. Opt. **41**, 7000 (2002).
[16] J. B. Hasted, *Physics of Atomic Collisions* (Butterworths, London, 1964).
[17] D. A. Church, J. Mod. Opt. **39**(2), 423 (1992).
[18] J. K. Kim, L. P. Theard, and W. T. Huntress Jr., Chem. Phys. Lett. **32**, 610 (1975); A. E. Roche, M. M. Sutton, D. K. Rohme, and H. I. Schiff, J. Chem. Phys. **55**, 5840 (1971).
[19] N. G. Adams and D. Smith, Chem. Phys. Lett. **105**, 604 (1984).
[20] M. G. Raizen, J. M. Gilligan, J. C. Berquist, W. M. Itano, and D. J. Wineland, Phys. Rev. A **45**, 6493 (1992).
[21] B. Roth, A. Ostendorf, H. Wenz, and S. Schiller, J. Phys. B **38**, 3673 (2005).
[22] B. Roth, P. Blythe, and S. Schiller (unpublished).
[23] T. Baba and I. Waki, J. Appl. Phys. **89**, 4592 (2001).
[24] T. Baba and I. Waki, Jpn. J. Appl. Phys., Part 1 **92**, 4109 (2002).
[25] T. Hasegawa and T. Shimizu, Phys. Rev. A **66**, 063404 (2002).
[26] U. Fröhlich, B. Roth, and S. Schiller, Phys. Plasmas **12**, 073506 (2005).

[27] *CRC Handbook of Chemistry and Physics* (Taylor and Francis, New York, 2002), p. 82.
[28] N. Vanhaecke, W. de Souza Melo, B. Laburthe Tolra, D. Comparat, and P. Pillet, Phys. Rev. Lett. **89**, 063001 (2005).
[29] C. Regal, C. Ticknor, J. L. Bohn, and D. Jin, Nature (London) **424**, 47 (2003).
[30] H. L. Bethlem, F. M. H. Crompvoets, R. T. Jongma, S. Y. T. van de Meerakker, and G. Meijer, Phys. Rev. A **65**, 053416 (2002); M. R. Tarbutt *et al.*, Phys. Rev. Lett. **92**, 173002 (2004).
[31] T. Junglen, T. Rieger, S. A. Rangwala, P. W. H. Pinske, and G. Rempe, Phys. Rev. Lett. **92**, 223001 (2004).
[32] J. D. Weinstein *et al.*, Nature (London) **395**, 395 (1998); **395**, 148 (1998).
[33] C. Wunderlich, G. Morigi, and D. Reiss, Phys. Rev. A **72**, 023421 (2005).
[34] P. O. Schmidt *et al.*, Science **309**, 749 (2005).